UNIVERSITY OF MINNESOTA
ST. ANTHONY FALLS HYDRAULIC LABORATORY

Project Report No. 331

Mathematical Modeling of STS Series 60 Turbine

by

Charles C. S. Song

and

X. Y. Chen

Prepared for

STS HydroPower Ltd.
Springfield, Ohio

July 1992

Minneapolis, Minnesota

Table of Contents

List of Figures

I. Introduction

Some existing hydro–turbines, especially small turbines, have not been extensively evaluated for their performance and possible upgrading. This may be at least partially due to the fact that the traditional means of evaluation, turbine testing, is quite expensive. The costs of design and evaluation can now be substantially reduced by taking advantage of the recent development of computational technology.

STS Hydropower Ltd. has contracted with the St. Anthony Falls Hydraulic Laboratory of the University of Minnesota to conduct a preliminary evaluation of the STS Series 60 Francis turbine using the recently developed mathematical modeling program. After completing the simulation based on the geometrical data initially furnished by STS Hydropower, new geometrical data were received and recalculations requested. The new geometry differs from the old one in that the trailing end has been lengthened and the edge sharpened and also a more streamlined leading edge given. Also, calculations of two flow conditions was requested: maximum efficiency condition and maximum output condition.

The work has now been completed and the results are described in this report. Some recommendations for future work to improve the efficiency of the turbine are also given.

II. The Mathematical Model Used

The turbulent flow model based on the weakly compressible flow theory and large eddy simulation approach recently developed at the St. Anthony Falls Hydraulic Laboratory has been used for this work. The governing equations are solved numerically using the finite volume approach and an explicit scheme. The model deals with unsteady fully three–dimensional turbulent flows with the compressibility and viscous effects accounted for. It can calculate time averaged as well as fluctuating quantities.

Other leading turbine flow models are based on Euler equations (nonviscous flow equations) which cannot directly calculate the energy loss. Therefore, the efficiency has to be estimated based on experience and assumptions. In contrast, this model gives the efficiency directly without any human judgment as long as the input data are correct. Being a weakly compressible unsteady flow model, this model can also be used to study acoustic and vibration problems if need arises.

III. Scope of Study

The main purpose of this study is to calculate the efficiency of the existing STS Series 60 turbine and to judge the feasibility of improving the design.

A model was set up using the geometrical data furnished by STS at the beginning of the project. However, after a run was completed, a new set of geometrical data were given by STS which differ with the initial data in a very substantial way. The trailing end of the blade was lengthened and the edge sharpened. The nose was also made sharper. A more detailed drawing of the guide vanes was given so that better estimates of the inflow angle became possible.

As a result of changed geometrical data, a new computational grid system was generated. Because of the increased sharpness of the blade, a much larger number of grids and, hence, larger amounts of computational time became necessary.

Two operating conditions: 1) the best efficiency condition and 2) the maximum gate opening condition were simulated. Since vibration was not the concern of this project, two flow passage channels were select4ed as the computational domain. Most other models use a single passage channel to keep the number of grids small. Our experience showed, however, that the two channel model gives the best overall performance as the speed of convergence was greatly increased.

The calculated velocity fields were used to determine if any flow separation existed. The calculated pressure distribution was integrated over the whole blade surface to produce torque and power output. The pressure distribution on the blade was also plotted to see if the design could be improved.

IV. Results of Simulation

The overall results in terms of power input–output and efficiencies are listed in Table 1. Note that the calculated efficiencies are slightly lower than the efficiencies given by STS and designated "experimental" in the table. Also to be noted is that the calculated power input and output are slightly higher than the values given by STS. This is probably due to a slight difference in the assumed inflow velocities. For mathematical modeling, the inflow velocity is assumed to be uniform, thereby ignoring the wake effect of the guide vanes.

TABLE 1

Main Characteristics of STS Series 60 Turbine

a. Best Efficiency Condition

	Experimental	Numerical
Input power P_{in} (hp)	None	3695.4
Output power P_{out} (hp)	3155.0	3385.2
Efficiency (%)	93.4	91.6

b. Maximum Output Condition

	Experimental	Numerical
Input power P_{in} (hp)	None	4576.5
Output power P_{out} (hp)	3712.0	3822.2
Efficiency (%)	87.1	83.5

A slight difference in input should not affect the calculated efficiency because the difference in Reynold's number is negligibly small. However, by ignoring the wake effect, the modeling may slightly overestimate the efficiency. This means that the actual efficiencies may be slightly lower than the calculated values. The more important consequence of not considering the wake effect is that the calculated oscillatory forces are not quite correct. It is well known that the spatial periodicity of the inflow velocity due to guide vane wake is a major source of oscillatory forces. However, this is out of the scope of the present study.

The grid system on a typical meridian plane is shown in Fig. 1. Note that JX indicates grid number in the general flow direction, JY is the grid number in the azimuthal direction, and JZ means the grid number along the thickness at the entrance.

The velocity vector fields relative to the rotating coordinate system on three typical X–Y surfaces for the best efficiency case are shown in Fig. 2(a), (b), and (c). The velocity vector fields on three meridial surfaces passing through the middle of a flow passage, on the suction side of a blade, and on the pressure side of a blade are shown in Fig. 3(a), (b), and (c), respectively. The pressure contour lines on the suction side and the pressure side of a blade are shown in Fig. 4(a) and (b), respectively. The number in these figures are pressure coefficient defined as

$$C_p = \frac{P - P_o}{\frac{1}{2} \rho U^2} \tag{1}$$

where C_p is the pressure coefficient, P is the pressure, P_o is a reference pressures, ρ is the density of fluid, and U is the speed of flow at the inlet.

Similar plots of velocity vector fields on X–Y surfaces for the case of maximum gate opening are shown in Fig. 5(a), (b), and (c). The corresponding plots for the three meridial surfaces are shown in Fig. 6 (a), (b), and (c). Finally the pressure distributions on the blade surfaces are shown in Fig. 7(a) and (b).

To observe more clearly the possible occurrence of flow separation, the velocity vector fields near the leading edge of the blade at JZ = 32 are enlarged and plotted in Fig. 8(a), for the case of best gate opening and in Fig. 8(b), for the case of maximum gate opening. These figures clearly show a significant leading edge separation in the case of maximum gate opening and a marginal amount of separation for the best case.

A few computer generated photographs of three–dimensional views of the STS series 60 turbine are also attached.

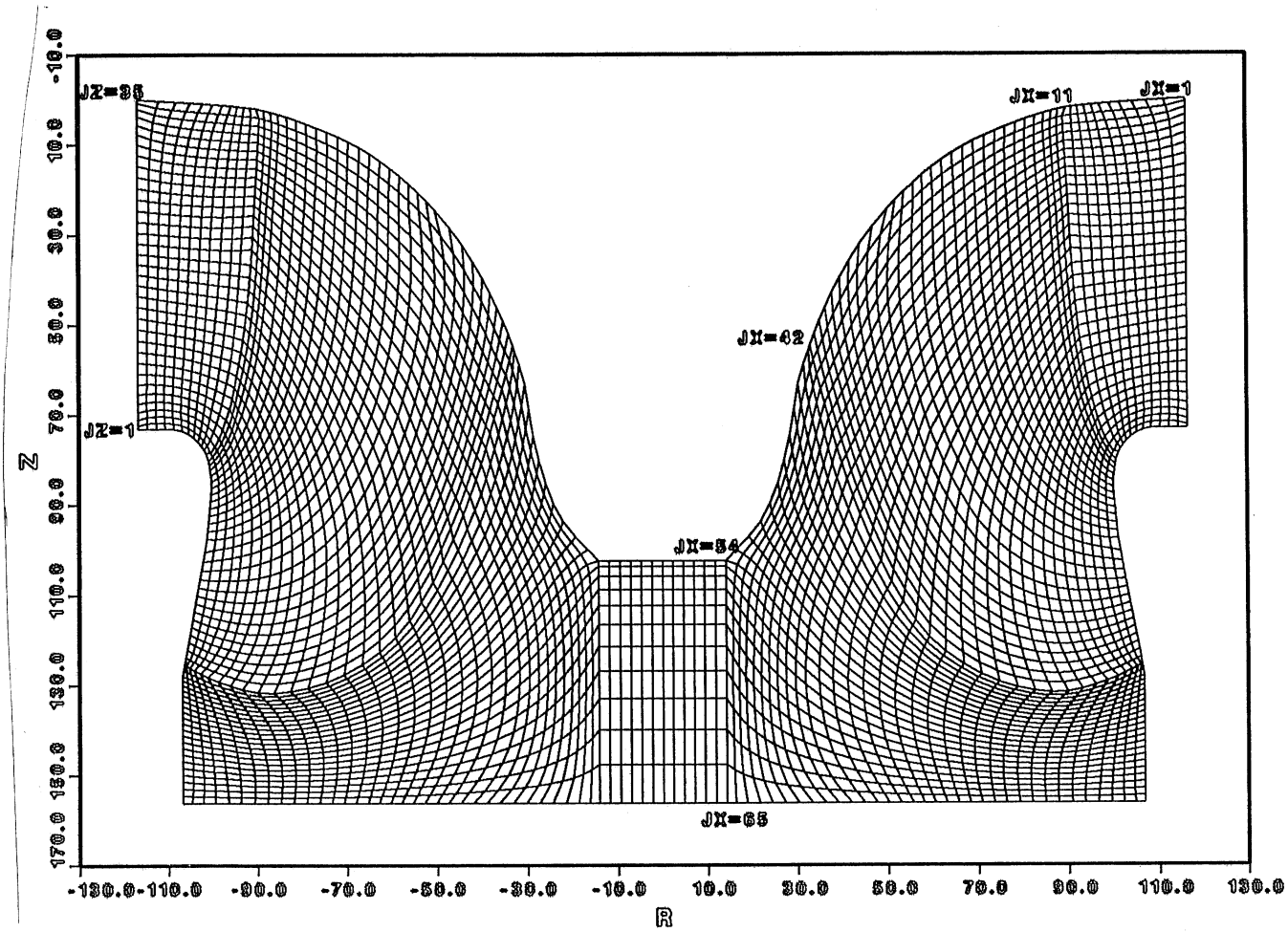

Figure 1 Grid generation for 3D turbine runner (STS Series 60 turbine).

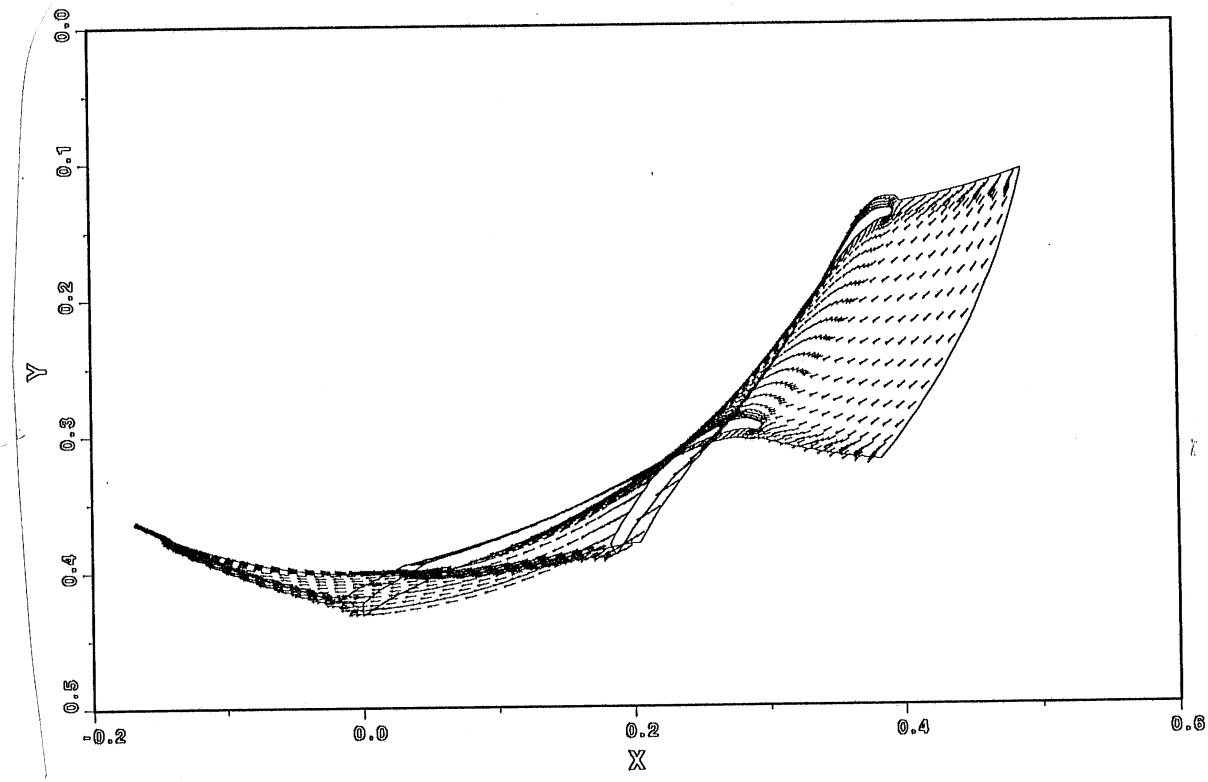

Figure 2a Modeled velocity field on X–Y plane (JZ=6, Vscale = 0.003). Best gate.

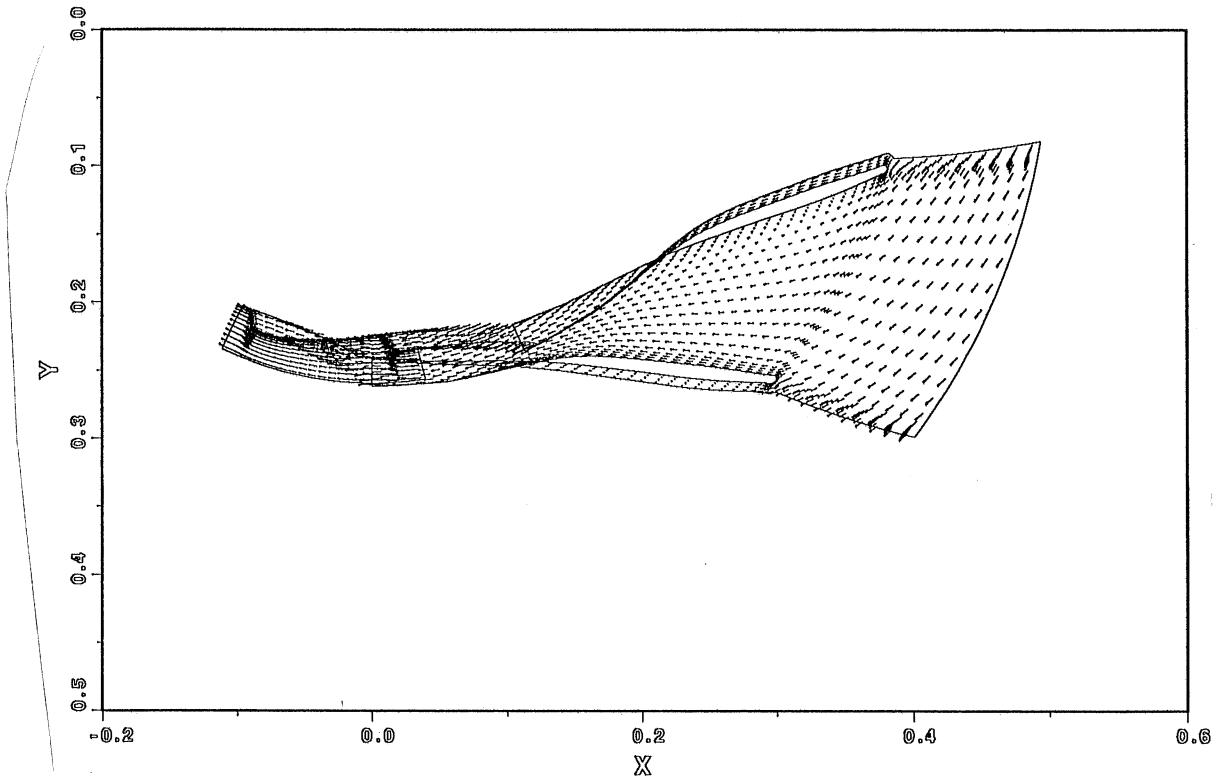

Figure 2b Modeled velocity field on X–Y plane (JZ=18, Vscale = 0.003). Best gate.

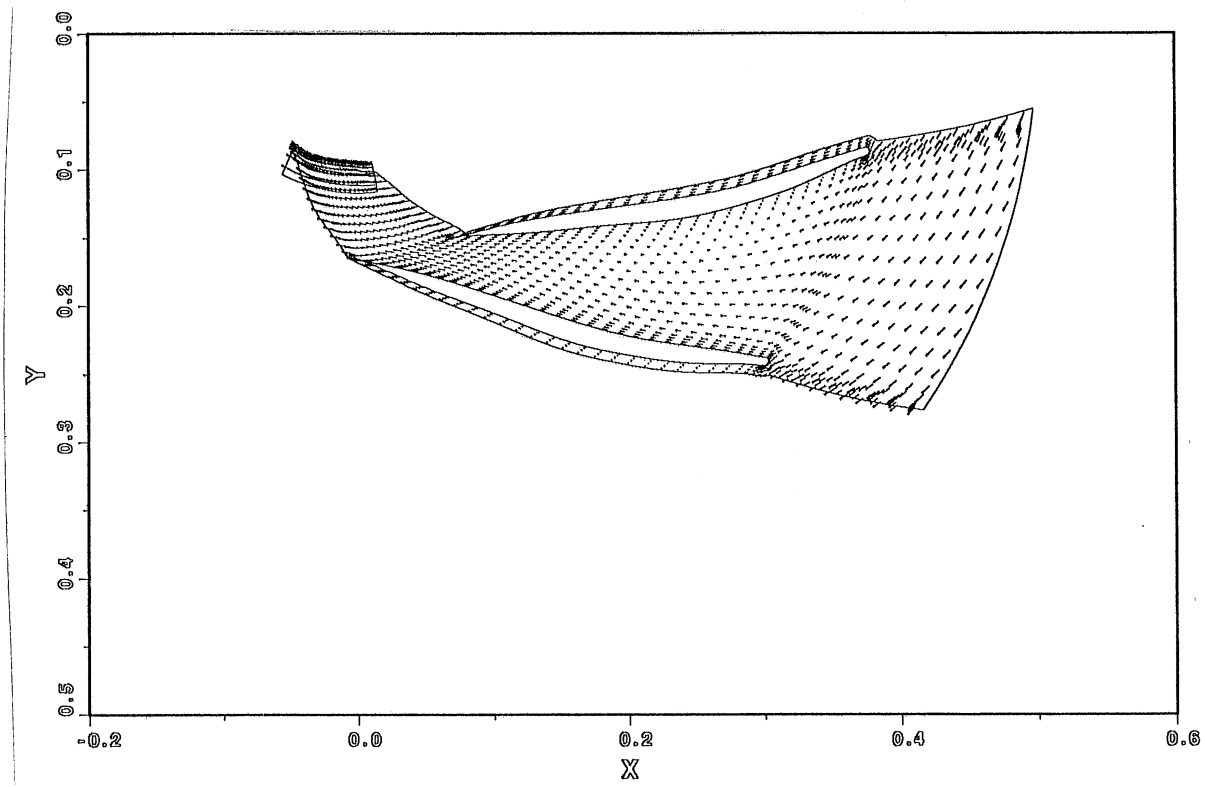

Figure 2c Modeled velocity field on X–Y plane (JZ=30, Vscale = 0.003). Best gate.

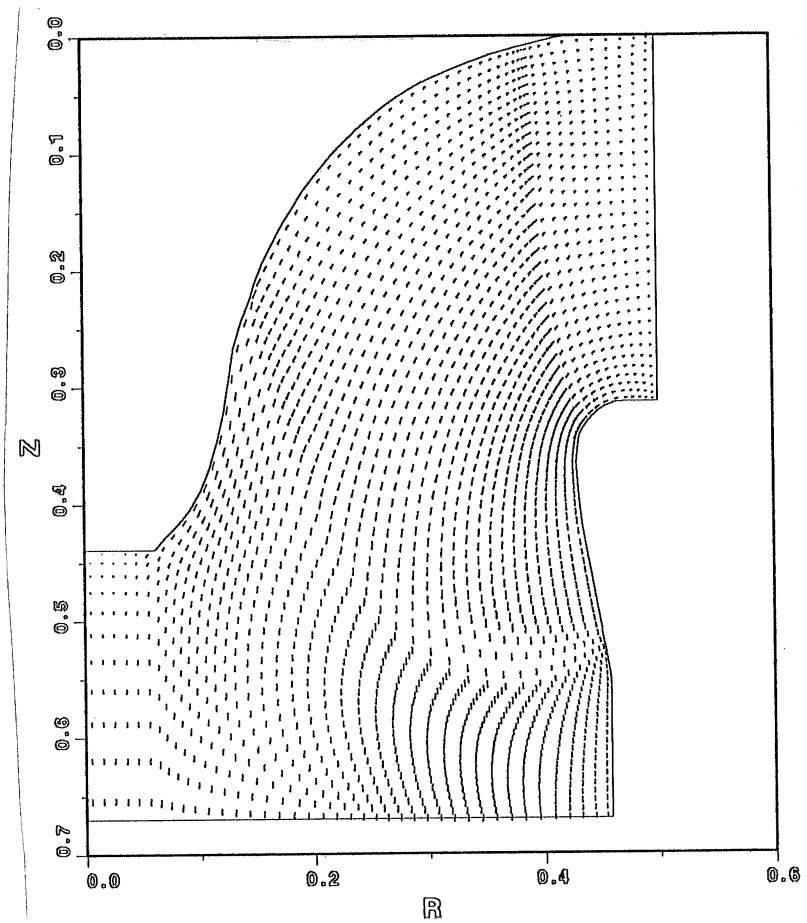

Figure 3a Modeled velocity field on R–Z plane (JY=19, Vscale = 0.003). Best gate: middle cross section.

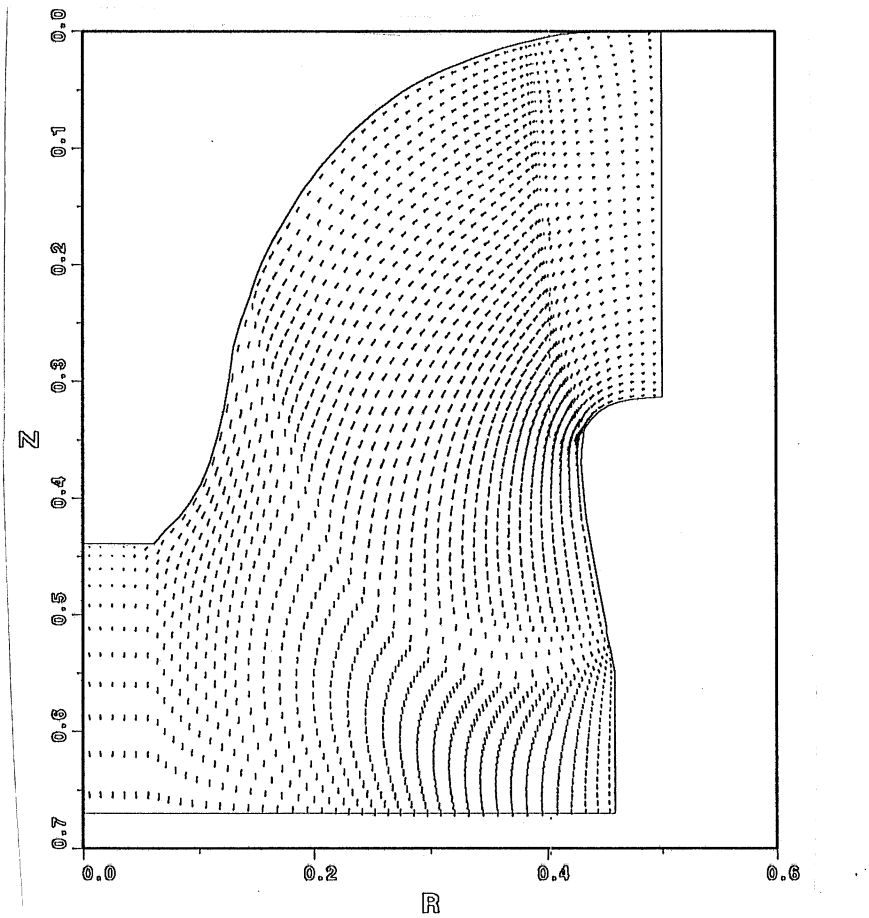

Figure 3b Modeled velocity field on R–Z plane (JY=29, Vscale = 0.003). Best gate: suction side.

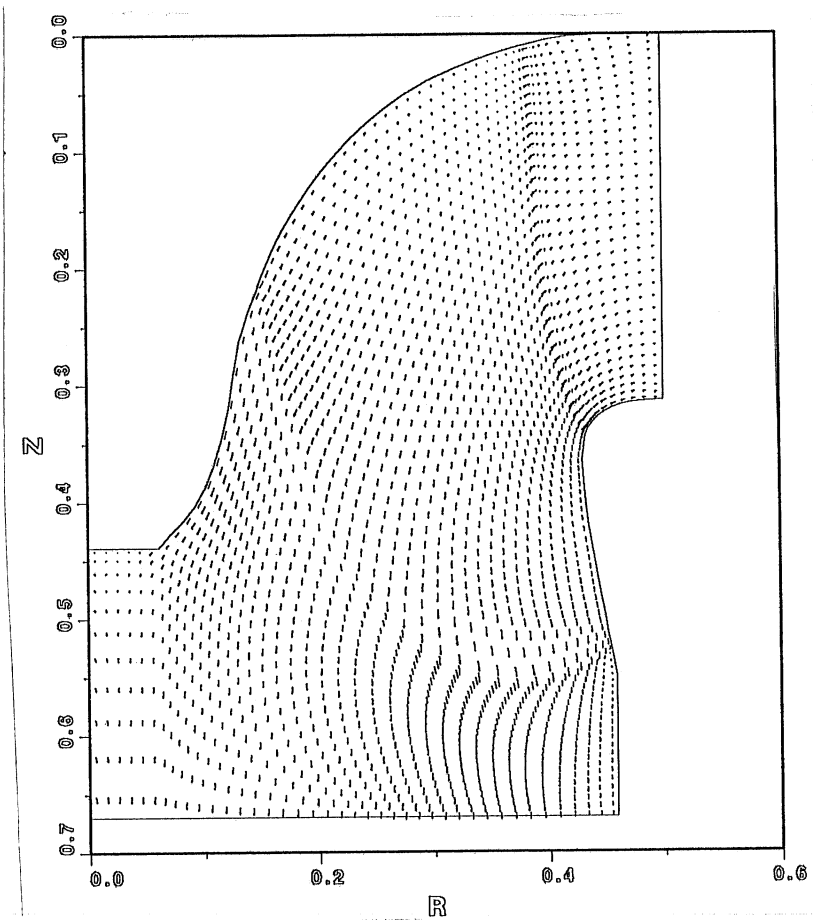

Figure 3c Modeled velocity field on R–Z plane (JY=34, Vscale = 0.003). Best gate: pressure side.

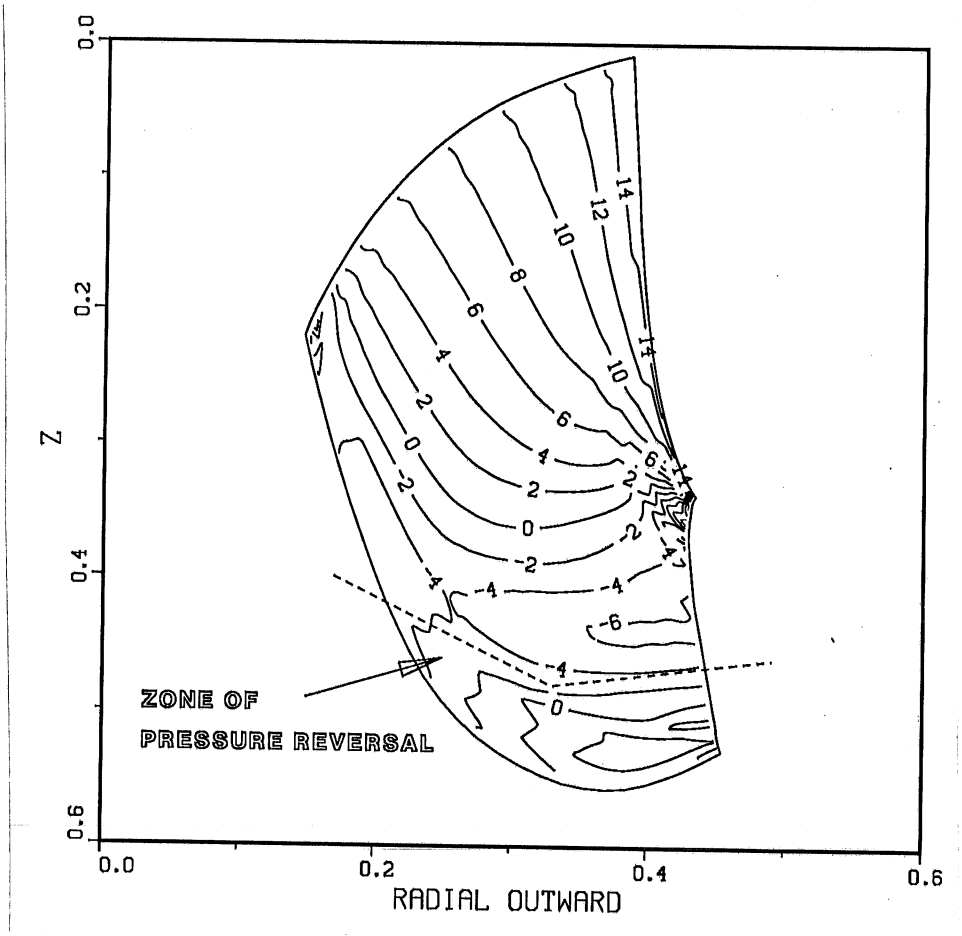

Figure 4a Pressure contour on blade (JY=29, Pre-scale = 1.00). Best gate: suction side.

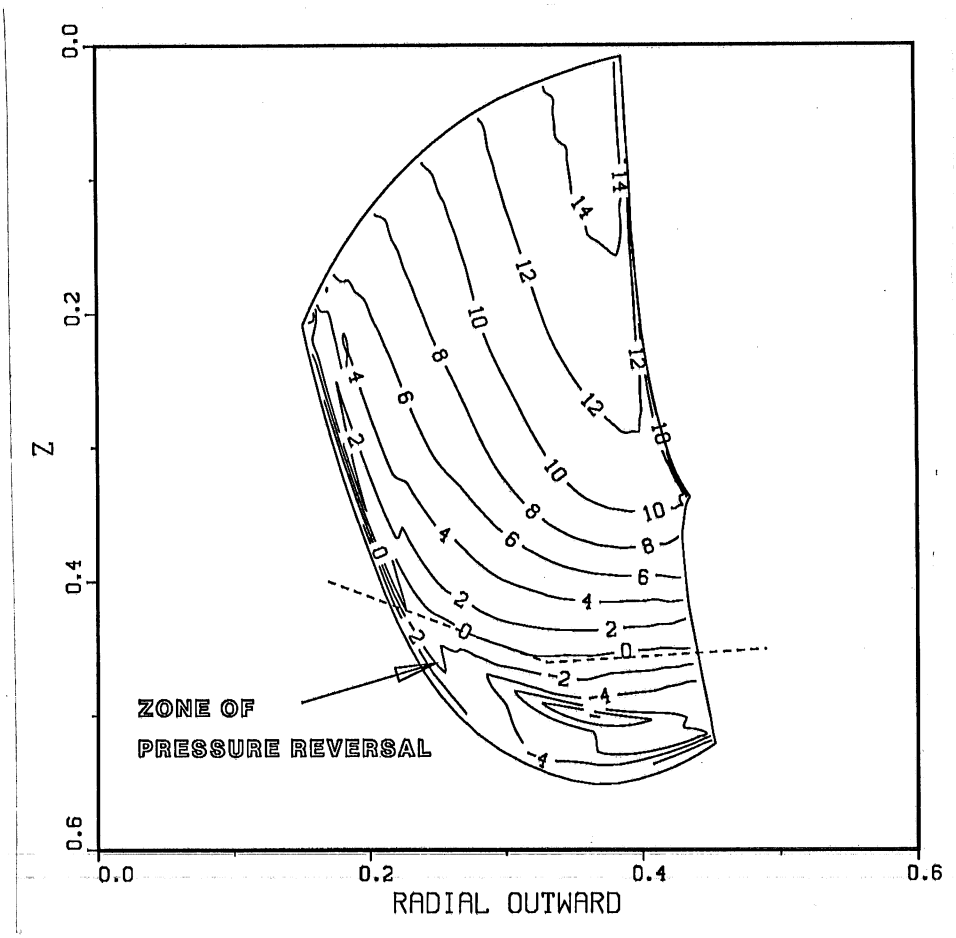

Figure 4b Pressure contour on blade (JY=34, Pre–scale = 1.00). Best gate: pressure side.

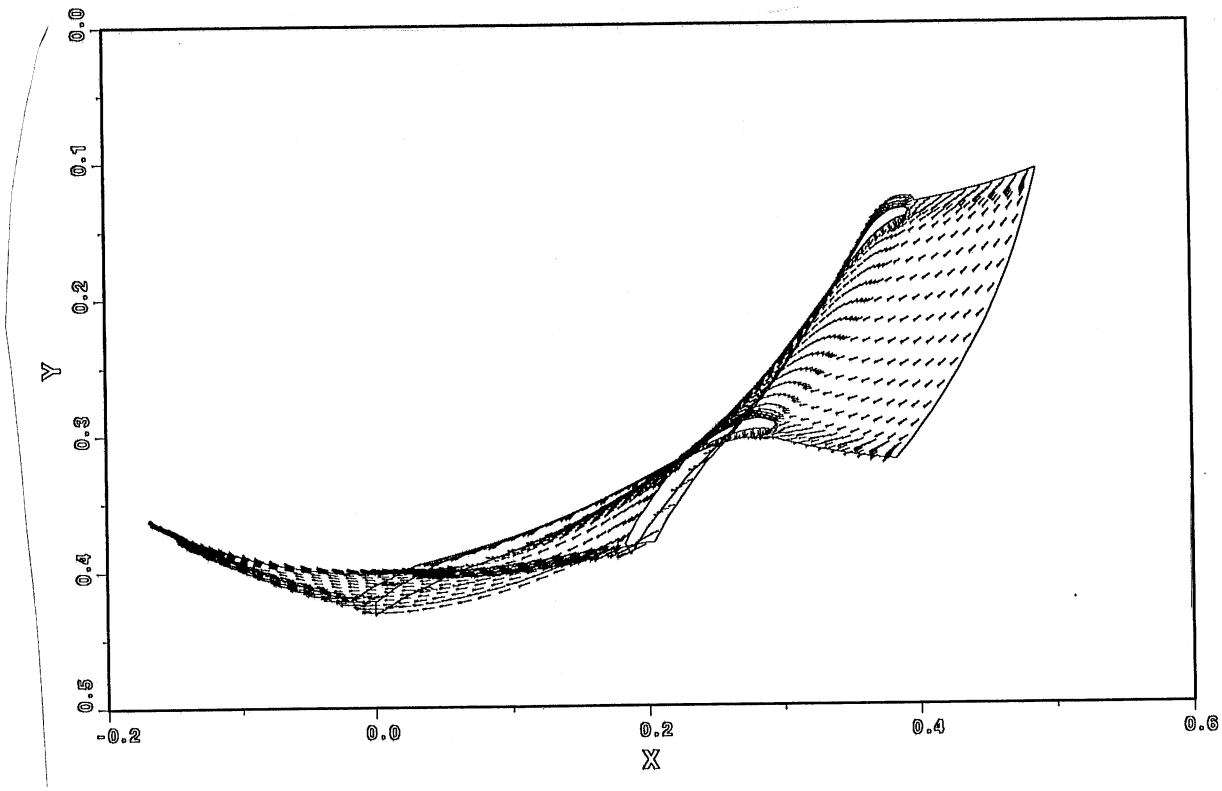

Figure 5a Modeled velocity field on X–Y plane (JZ=6, Vscale = 0.003). Maximum gate.

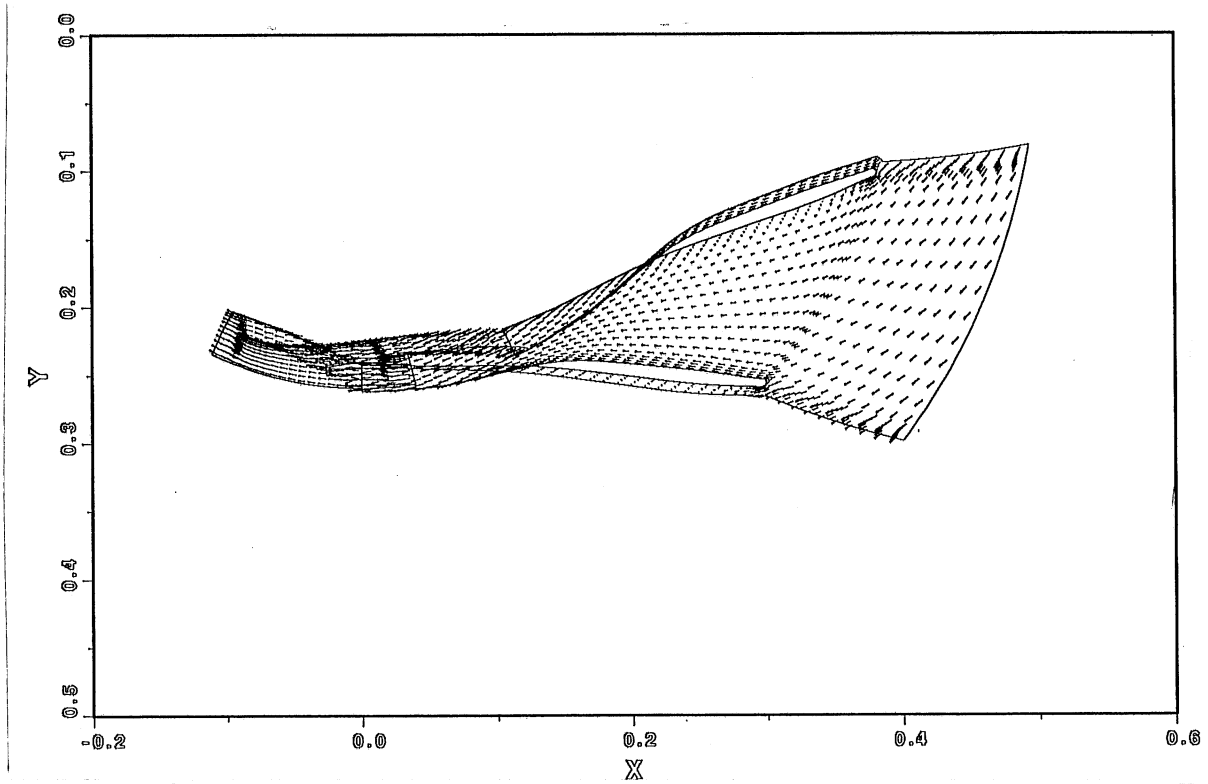

Figure 5b Modeled velocity field on X–Y plane (JZ=18, Vscale = 0.003). Maximum gate.

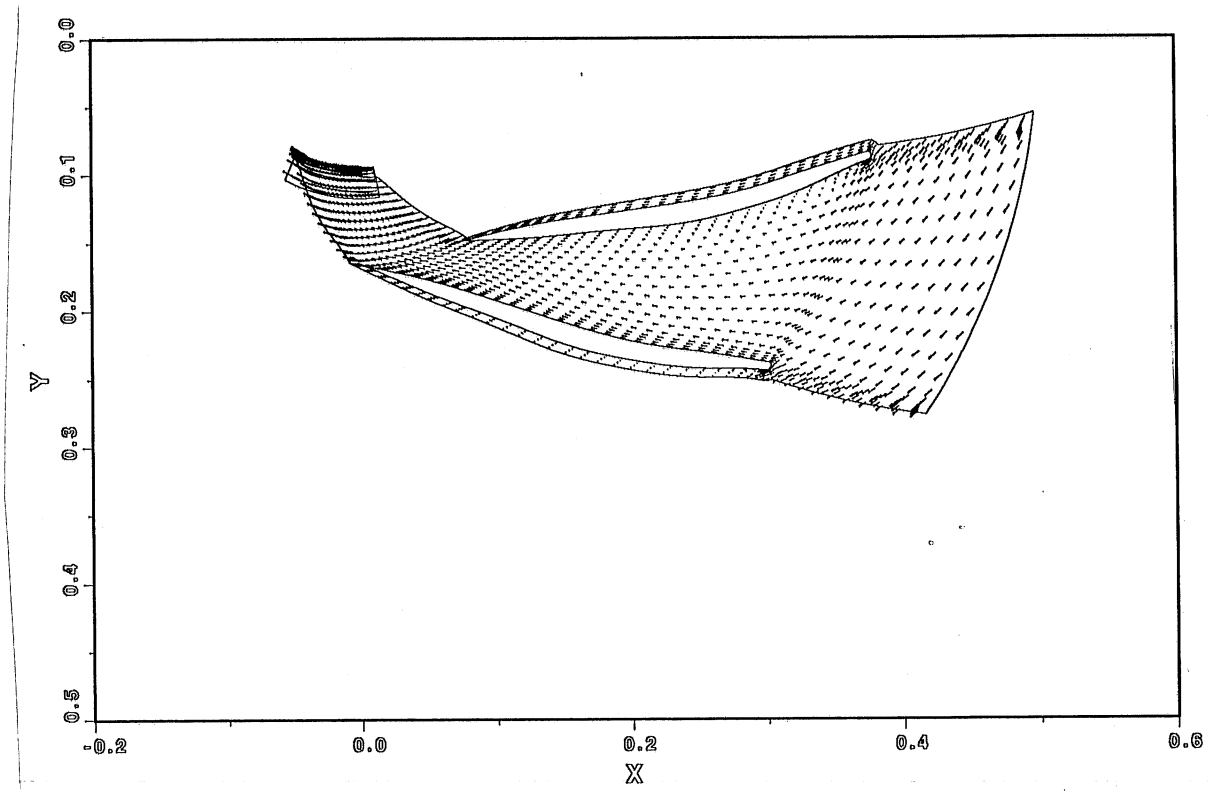

Figure 5c Modeled velocity field on X–Y plane (JZ=30, Vscale = 0.003). Maximum gate.

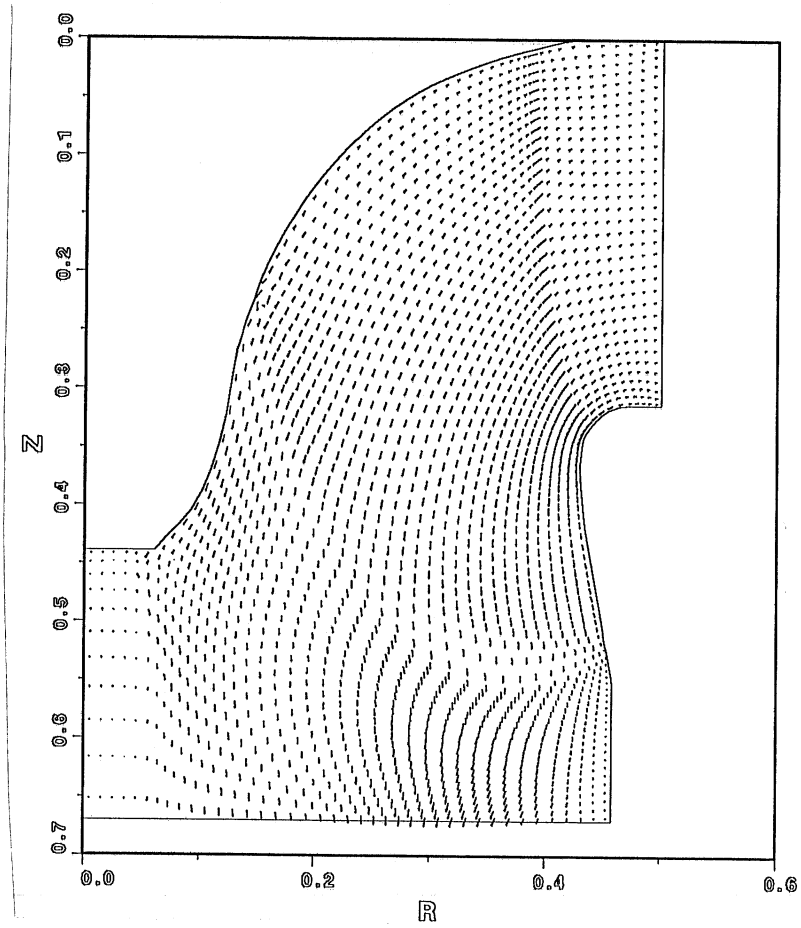

Figure 6a Modeled velocity field on R–Z plane (JY=19, Vscale = 0.003). Maximum gate: middle cross section.

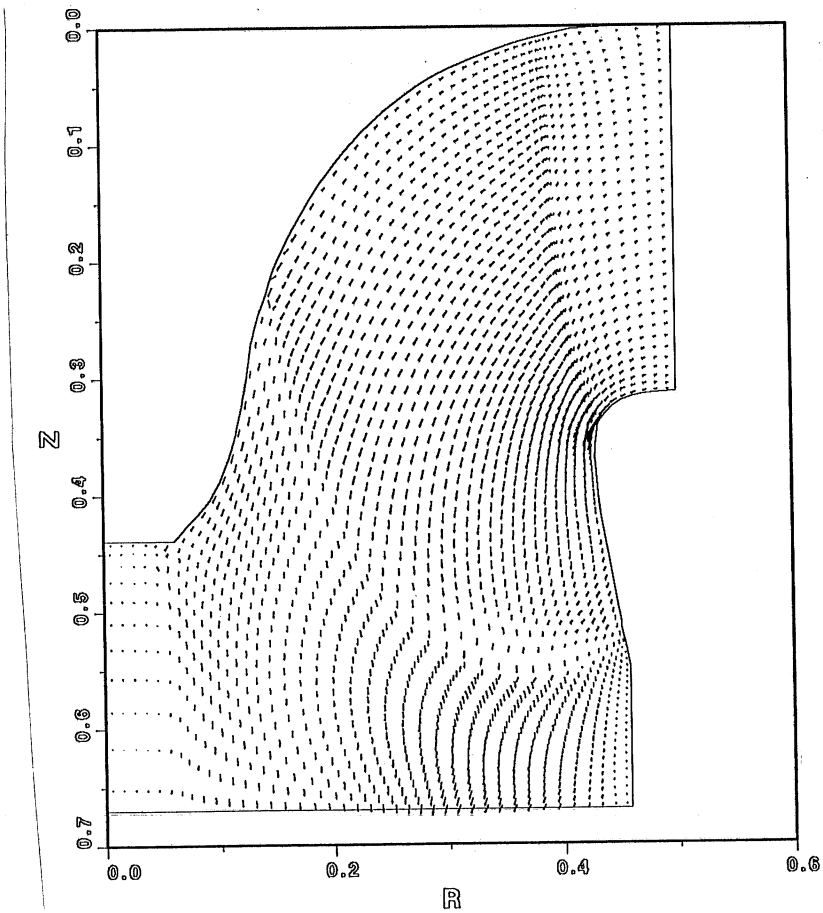

Figure 6b Modeled velocity field on R–Z plane (JY=29, Vscale = 0.003). Maximum gate: suction side.

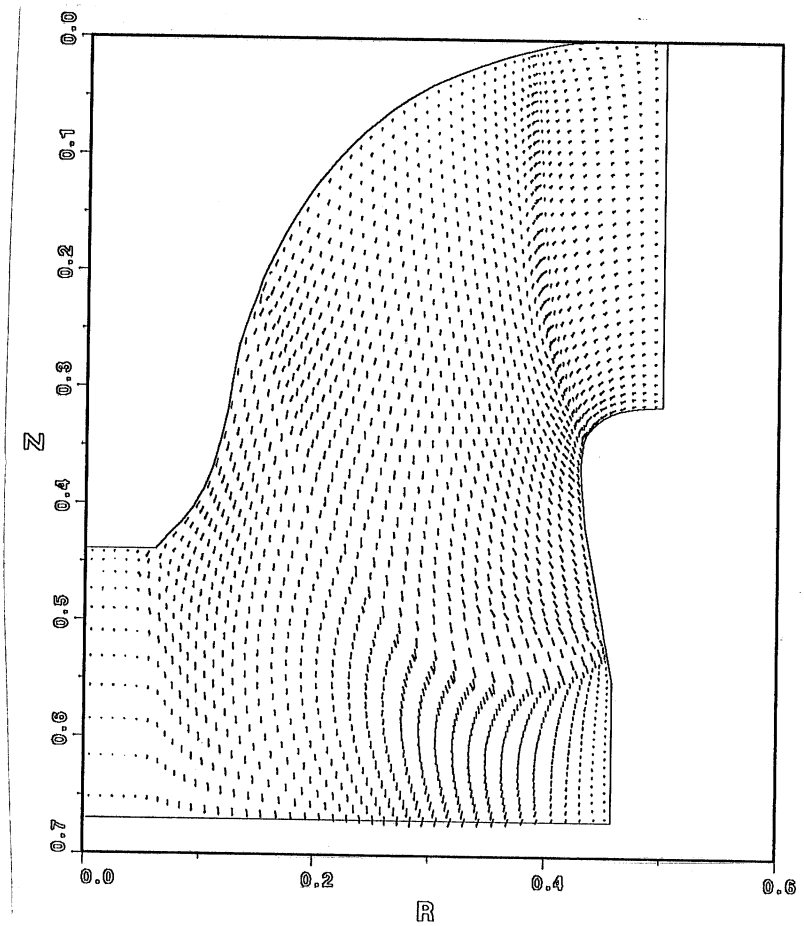

Figure 6c Modeled velocity field on R–Z plane (JY=34, Vscale = 0.003). Maximum gate: pressure side.

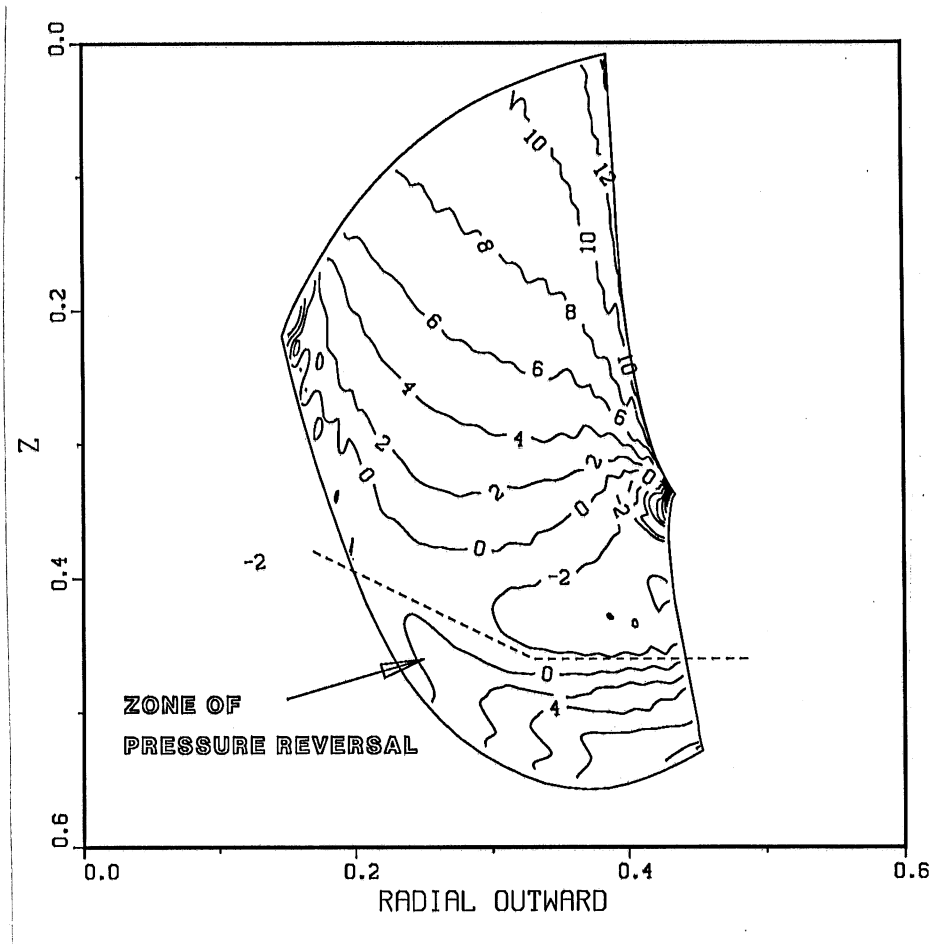

Figure 7a Pressure contour on blade (JY=29, pre-scale = 1.00). Maximum gate: suction side.

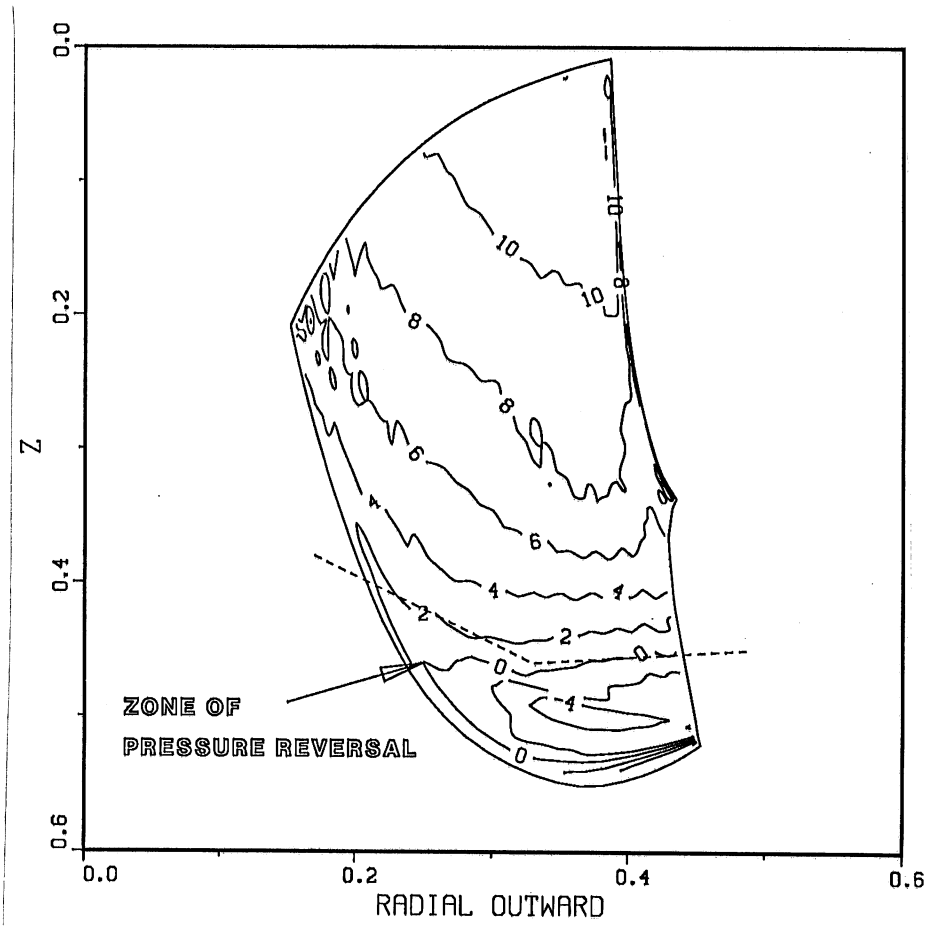

Figure 7b Pressure contour on blade (JY=34, pre-scale = 1.00). Maximum gate: pressure side.

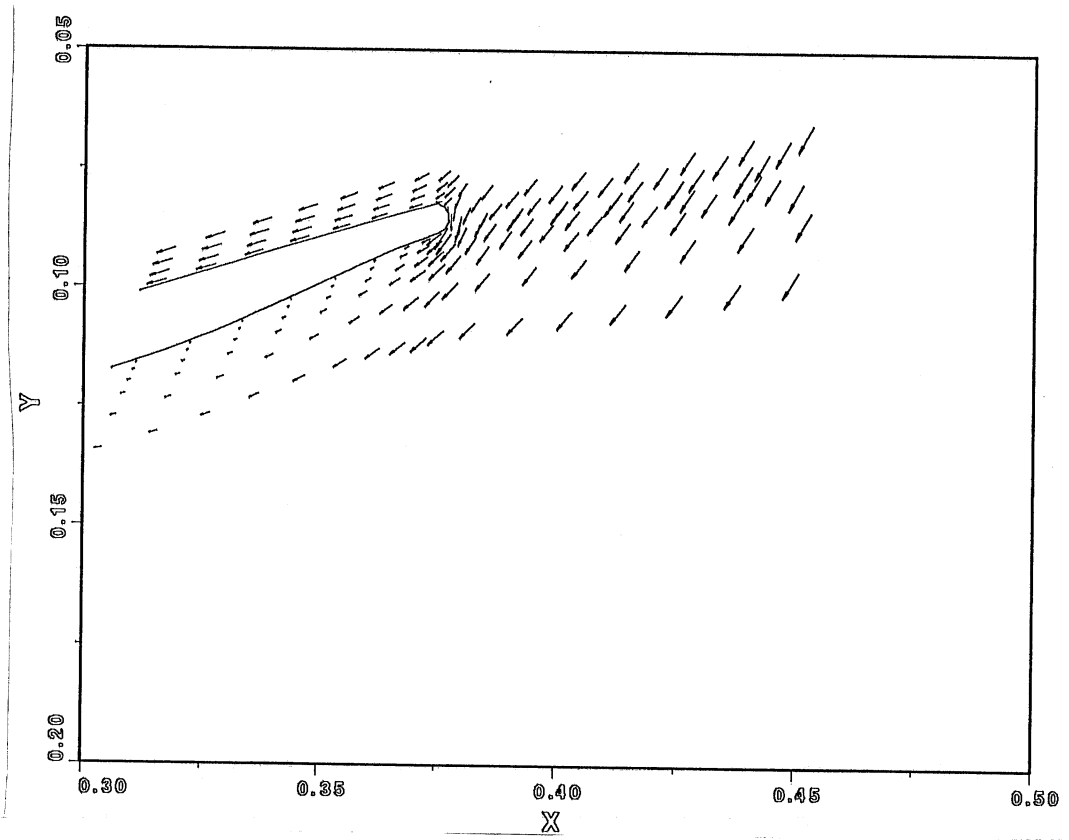

Figure 8a Modeled velocity field on X–Y plane (JZ=32, Vscale = 0.003). Leading edge: best gate.

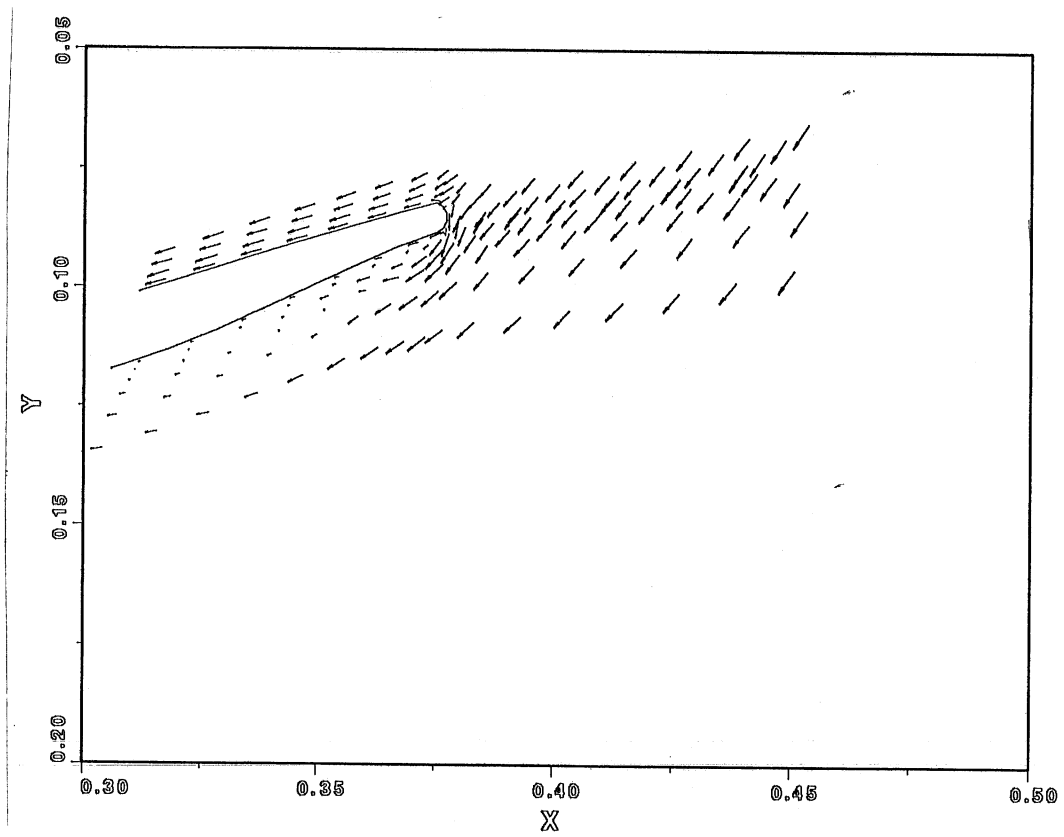

Figure 8b Modeled velocity field on X–Y plane (JZ=32, Vscale = 0.003). Leading edge: maximum gate.

V. Discussions and Recommendations

The computed efficiencies for both cases are slightly lower but very close to the rated value as indicated in Table 1. Both the rated and the calculated efficiencies are substantially below achievable values. According to literature, it is not unusual for a Francis turbine to achieve 95 percent or higher efficiency.

Detailed analysis of the numerical results suggests that there are two possible areas of improvement. These are related to (1) the leading edge flow separation and (2) the pressure reversal near the trailing end and the hub. These are separately described below.

(1) Leading edge separation

As clearly shown in Fig. 8(b) there is a short separation bubble on the suction side near the leading edge. Consequently, a fairly high pressure zone is generated near the reattachment point causing a reduction in lift. One of the reasons why the efficiency of the maximum gate opening case is lower than the best efficiency case is undoubtedly due to the leading edge separation. The leading edge flow separation is sensitive to the angle of attack and the profile near the leading edge.

(2) Pressure reversal

Ideally, the pressure on the suction side should be lower than the pressure at the corresponding location the the pressure side. The present calculation shows that there is a significant area near the tailing edge and the hub as shown in Fig. 4 and Fig. 7 where the pressure is higher on the suction side than that of the pressure side. In effect, the role of two surfaces are reversed causing reductions in lift force and efficiency.

The pressure reversal is apparently due to insufficient camber in the area below the dotted line shown in Figs. 4 and 7. A possible solution to this problem is to increase the camber by increasing the skewness.

Based on the results of this modeling work and the discussions given above, the following future work to increase the efficiency of STS Series 60 turbines is recommended.

(1) Modify the blade profile near the leading edge to eliminate or reduce the leading edge separation.

(2) Increase the camber in the downstream half of the blade by increasing the skewness of the blade.